JACS
JOURNAL OF THE AMERICAN CHEMICAL SOCIETY
Article
pubs.acs.org/JACS

Direct C−C Coupling of CO_2 and the Methyl Group from CH_4 Activation through Facile Insertion of CO_2 into Zn−CH_3 σ-Bond

Yuntao Zhao,[†] Chaonan Cui,[†,‡] Jinyu Han,[†] Hua Wang,[†] Xinli Zhu,*[,†] and Qingfeng Ge*[,†,‡]

[†]Collaborative Innovation Center of Chemical Science and Engineering, School of Chemical Engineering and Technology, Tianjin University, Tianjin 300072, China

[‡]Department of Chemistry and Biochemistry, Southern Illinois University, Carbondale, Illinois 62901, United States

Supporting Information

ABSTRACT: Conversion of CO_2 and CH_4 to value-added products will contribute to alleviating the green-house gas effect but is a challenge both scientifically and practically. Stabilization of the methyl group through CH_4 activation and facile CO_2 insertion ensure the realization of C−C coupling. In the present study, we demonstrate the ready C−C coupling reaction on a Zn-doped ceria catalyst. The detailed mechanism of this direct C−C coupling reaction was examined based on the results from density functional theory calculations. The results show that the Zn dopant stabilizes the methyl group by forming a Zn−C bond, thus hindering subsequent dehydrogenation of CH_4. CO_2 can be inserted into the Zn−C bond in an activated bent configuration, with the transition state in the form of a three-centered Zn−C−C moiety and an activation barrier of 0.51 eV. The C−C coupling reaction resulted in the acetate species, which could desorb as acetic acid by combining with a surface proton. The formation of acetic acid from CO_2 and CH_4 is a reaction with 100% atom economy, and the implementation of the reaction on a heterogeneous catalyst is of great importance to the utilization of the greenhouse gases. We tested other possible dopants including Al, Ga, Cd, In, and Ni and found a positive correlation between the activation barrier of C−C coupling and the electronegativity of the dopant, although C−H bond activation is likely the dominant reaction on the Ni-doped ceria catalyst.

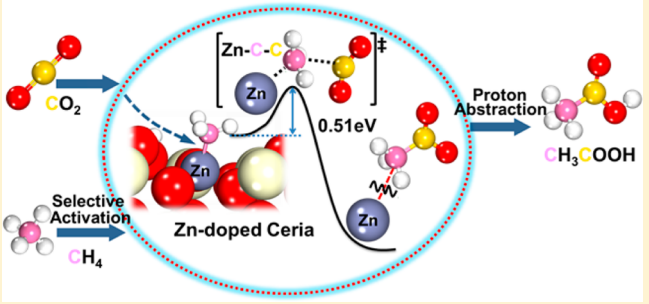

INTRODUCTION

Increased consumption of fossil fuels since the industrial revolution has resulted in a steady increase of the CO_2 concentration in the atmosphere. CO_2 is the main contributor to global warming which poses a devastating threat to the sustainability and prosperity of society.[1] Carbon capture and storage (CCS), once implemented, could stabilize the atmospheric CO_2 level, but the high cost hinders its deployment.[2] Conversion of CO_2 to high energy density and other high value products addresses both climate change and fossil fuel shortage. Due to the inertness of CO_2, its conversion requires energy inputs in various forms, including thermal, electrical, photo, or more energetic reactants. For example, electricity is used in electrochemical reduction,[3] solar energy in photoreduction reaction,[4] hydrogen in methanol synthesis and methanation reaction[5] as well as CH_4 in the re-forming reaction.[6] Abundant shale gas reserves make CH_4 a viable source of both energy and hydrogen for CO_2 conversion.

Most of the previous studies focused on the traditional syngas route, i.e., using CO_2 and CH_4 to produce CO and hydrogen, followed by either methanol synthesis or Fischer−Tropsch processes to produce high value chemicals. The syngas route has the advantage of easy integration with the existing technology, but the syngas production from CO_2 re-forming of CH_4 is energy-intensive. There have been attempts at directly synthesizing C_2 hydrocarbons from CH_4 and CO_2 using a La_2O_3/γ-Al_2O_3 catalyst, but the results showed that both carbon atoms in the product came from CH_4.[7]

Recently, Banerjee and co-workers identified a sustainable C−C bond formation route through the reaction of CO_2 with deprotonated C−H bonds, which is simple and applicable to economical production.[8] However, facile C−C bond formation from CO_2 and CH_4 is still challenging and potentially beneficial, since coconversion of CO_2 and CH_4 into acetic acid has an atom economy of 100%, in which the formation of acetate species (CH_3COO^*) through C−C coupling is dominant.[9] The reaction has been accomplished experimentally under homogeneous conditions, catalyzed by vanadium complexes[10] and $Pd(OAc)_2/Cu(OAc)_2/K_2S_2O_8/CF_3COOH$,[11] but product separation at the end of the reaction presented a great challenge. So far, many heterogeneous catalysts, such as Cu/Co-based metal oxide,[12] Pd/C and Pt/Al_2O_3,[13] $V_2O_5-PdCl_2/Al_2O_3$,[14] Pd/SiO_2 and Rh/SiO_2,[15] have been attempted for the coconversion of CO_2 and CH_4 into acetic acid. The formation of acetic acid under plasma conditions was also investigated.[16] In each case, however, the

Received: April 29, 2016
Published: July 23, 2016

DOI: 10.1021/jacs.6b04446
J. Am. Chem. Soc. 2016, 138, 10191−10198

result shows a broad product distribution, poor selectivity, and a low yield of acetic acid. This could be a result of the failure to stabilize the methyl radical and a high C−C coupling barrier.

Interestingly, the methyl radical could be successfully stabilized on metal sites of bulky ligands and carboxylation could be realized through CO_2 inserting into M-CH_3 bond in organic synthesis.[17] For example, Darensbourg and co-workers reported the reaction of CO_2 insertion into *cis*-$CH_3W(CO)_5^-$.[17b] They found that at a low CO_2 pressure, the insertion step occurs over days along with the decomposition of the product. Johansson et al. used approximately 30 equiv of CO_2 in a coupling reaction with $PCP^{(tBu)}Pd-CH_3$ (PCP = 2,6-bis[(di-*tert*-butylphosphino)methyl]phenyl) and tested the product $PCP^{(tBu)}PdOAc$ using NMR.[17c] In a recent study, inserting CO_2 into (PCP)Ni−CH_3 was shown to have a very high barrier of 1.32 eV (all energies involved in this article are converted into eV for comparison).[17f] Efficient formation of C−C bond is the major challenge for producing compounds using CO_2. Although these CO_2 insertion reactions are slow, their realization in homogeneous synthesis provides inspiration for implementing a similar process under heterogeneous conditions.

Recently, selective activation of CH_4 has been achieved on zinc-exchanged MFI-type and H-ZSM-5 zeolites under heterogeneous condition.[9a,18] The methyl from CH_4 dissociation was stabilized on the zinc site in the form of $-[ZnCH_3]^+$ species, observed by IR and NMR. C−C bond formation through CO_2 insertion into the M−C σ-bond is expected to be the key step in a heterogeneously catalyzed C−C coupling reaction. A theoretical study on the Au-ZSM-5 catalyst showed that C−C coupling could be achieved by CO_2 insertion into the Au−CH_3 bond; however, the coupling barrier of 2.88 eV makes the reaction almost impossible in practice.[19] Importantly, the C−C bond could form through insertion of CO_2 into the organozinc reagents catalyzed by $Pd(OAc)_2$, $[Ni(PCy_3)_2]_2(N_2)$, $Ni(acac)_2$ or in the presence of $MgCl_2$ or LiCl in the solvent.[20] Also, CO_2 insertion into the Zn−H bond could be readily accomplished.[21]

Herein, we report the use of a Zn-doped ceria as a catalyst to facilitate the coupling of CO_2 and methyl from CH_4 activation through insertion of CO_2 into the Zn−CH_3 bond. The ability of Zn^{2+} in stabilizing CH_3 to hinder further oxidation[9a,18] and the ceria in activation of CO_2 is key to implement the reaction.[22] We use the density functional theory (DFT) method to track the elementary steps and elucidate the reaction mechanism. We showed that the C−C coupling reaction is facile and desorption of acetic acid following the formation of the acetate species depends strongly on the reaction environment. We also explored other metals as dopant in a ceria-based catalyst and found a correlation between the barrier of the coupling reaction and the electronegativity.

METHODS

Spin-polarized calculations were performed at the DFT+*U* level using the Vienna ab initio simulation package (VASP).[23] In order to properly localize the Ce 4f states, the Hubbard-like *U* correction has been used in combination with the Perdew−Burke−Ernzerhof (PBE) functional.[24] The effective *U* parameter is defined as the difference between the Coulomb *U* and the exchange *J* terms. A value of 5.0 eV was set for the *U* parameter, following our previous work,[25] and consistent with the values used by others.[26] Projector-augmented wave (PAW) potentials were used to describe the effective cores.[27] The valence electrons of all atoms were expanded in a plane wave basis set with a cutoff energy of 400 eV. The atomic structures were relaxed using either the conjugate gradient algorithm or the quasi-Newton scheme as implemented in the VASP code until the forces were less than 0.02 eV/Å for all unconstrained atoms.

We chose the ceria (111) surface and used a slab consisting of 48 O atoms and 24 Ce atoms. Those atoms were distributed in three O−Ce−O trilayers and separated by a vacuum space of 15 Å. Zn-doped ceria (111) surface was constructed by substituting one Ce atom with a Zn atom in the supercell, and oxygen vacancies in the surface layer were created by removing two O atoms in the para-position next to the replaced Ce atom. The atoms in the bottom layer were fixed at their corresponding bulk positions, and the top two layers together with the adsorbates were allowed to relax during the calculation. A $(2 \times 3 \times 1)$ k-point grid was used to generate the K-points.

The adsorption energy was defined as

$$E_{ads} = E_{(adsorbate/slab)} - E_{(adsorbate)} - E_{(bare\ slab)} \quad (1)$$

where $E_{(adsorbate/slab)}$, $E_{(adsorbate)}$, and $E_{(bare\ slab)}$ represent the total energies of surface slab with the adsorbate, the isolated adsorbate molecule, and the optimized bare slab, respectively. A positive value corresponds to an endothermic process, whereas a negative value indicates the process is exothermic. Normal mode harmonic analysis was applied to stable and transition states. The transition state was confirmed with only one imaginary mode.

RESULTS AND DISCUSSION

Bulk and Zn-Doped Ceria. The optimized lattice parameter of bulk ceria is 5.437 Å, consistent with the experimental values[28] and previous computational studies.[26b,29] We also calculated the dissociative adsorption energy of methane on pure ceria (111) surface and obtained a value of −0.78 eV, in good agreement with the previous reports.[26a,30] The surface slab was modeled using a (2×4) surface supercell. The Zn-doped ceria was constructed by replacing a Ce atom with one Zn atom and removing two oxygen atoms in the para-position next to the replaced Ce atom, as shown in Figure 1.

We calculate the energy of oxygen vacancy formation (E_f) according to the following formula:

$$E_f = E_{(Zn_xCe_{1-x}O_{2-\delta})} + E_{(O_2)} - E_{(Zn_xCe_{1-x}O_2)} \quad (2)$$

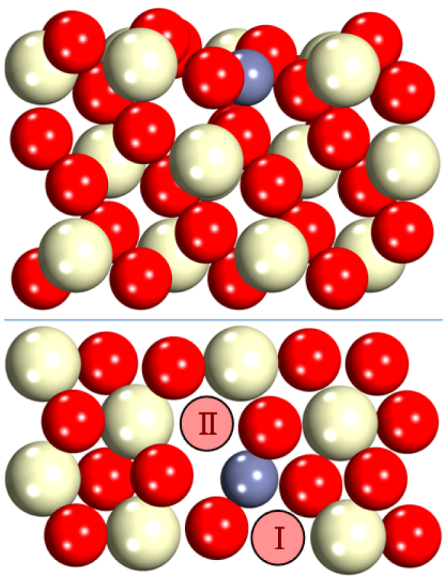

Figure 1. Relaxed structure of the Zn-doped ceria surface: side view (upper) and top view (lower). Surface and subsurface oxygen vacancies are labeled as I and II, respectively. In this and subsequent figures, Ce is ivory, O is red, and Zn is purple.

DOI: 10.1021/jacs.6b04446
J. Am. Chem. Soc. 2016, 138, 10191−10198

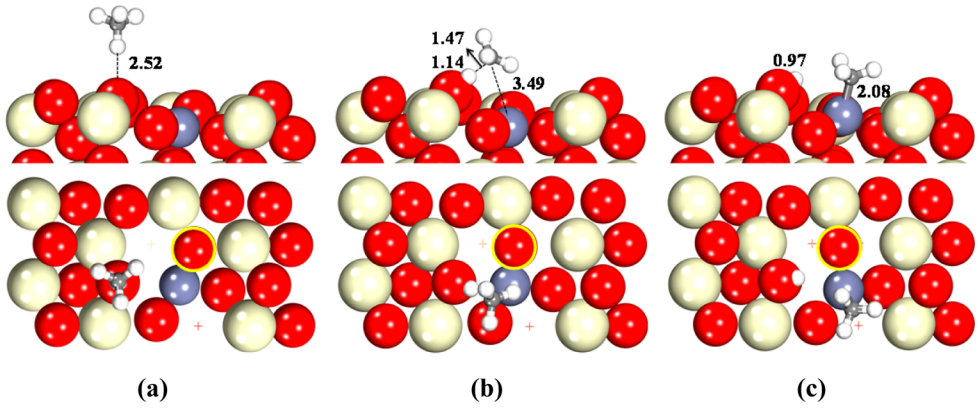

Figure 2. Side view (upper) and top view (lower) of initial (a), transition (b), and final (c) states for dissociative adsorption of CH_4. C and H are marked as gray and white. Distances of H−O, H−C, and C−Zn are in Å. O atom with the yellow circle (the same label in the following figures) moves slightly toward the subsurface oxygen vacancy.

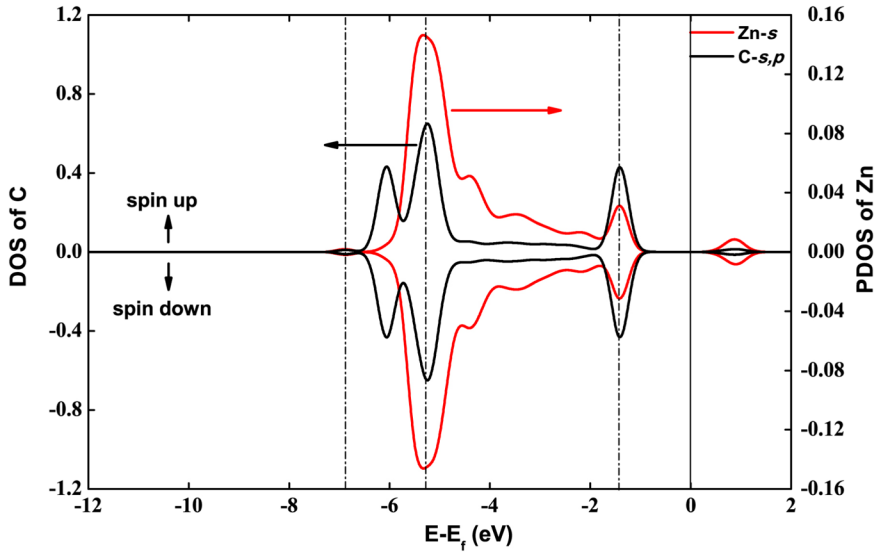

Figure 3. PDOS of Zn (red line) and DOS of C (black line). The Fermi level is indicated by a solid line, and the dotted dash lines represent the overlaps between Zn and C.

where $E_{(Zn_xCe_{1-x}O_{2-\delta})}$, $E_{(O_2)}$, and $E_{(Zn_xCe_{1-x}O_2)}$ are the energies of Zn-doped ceria slab with the oxygen vacancies, gas-phase O_2, and the slab without oxygen vacancies after doping Zn into the lattice, respectively. The calculated vacancy formation energy is 1.21 eV, much lower than that of the pure ceria (111). We point out that the value of 1.21 eV is calculated on the basis of direct desorption of oxygen into the gas phase. The creation of oxygen vacancy is expected to be more facile if assisted by reducing regents such as H_2 or CO, as shown in the case of In_2O_3.[31] The results demonstrated that doping Zn in CeO_2 facilitates oxygen vacancy formation.

Dissociative Adsorption of CH_4. The optimized structure of dissociative adsorption of CH_4 is depicted in Figure 2.

Methane is physisorbed on the surface, as shown in Figure 2a, with the H of CH_4 pointing to the surface O at a distance of 2.52 Å and adsorption energy of −0.04 eV. The physisorbed CH_4 is the initial state for C−H bond activation. In the transition state shown in Figure 2b, the C−H bond is elongated to 1.47 Å from 1.09 Å of the free CH_4 molecule. After overcoming a small barrier of 0.36 eV, the methyl and H atom became coadsorbed on the surface. In the final state, the methyl group binds to the zinc site through a Zn−C bond of 2.08 Å. The combination of methyl with a metal ion prevented its further dehydrogenation or oxidation and made it susceptible for the subsequent C−C coupling reaction.[9a,32] On the Zn-doped ceria surface, the H atom becomes a proton by forming a O−H bond with a bond length of 0.97 Å. The formation of the OH species generated a surface Brønsted acid site. The hydroxyl tilts toward the zinc center. At the same time, one of the oxygen atoms (marked with yellow circle in Figure 2) next to the zinc site moved toward the subsurface oxygen vacancy site. The surface methyl species has its Zn−C bond tilted toward the oxygen vacancy. The three C−H bonds of the surface methyl species remain at the same length of 1.10 Å, close to the gas phase value of 1.09 Å. The dissociative CH_4 adsorption energy on the surface is −0.53 eV with respect to the free molecule and bare slab.

To further understand the interaction between methyl species and the surface, we analyzed the projected density of states of Zn and C and plotted the results in Figure 3.

As shown in Figure 3, significant overlaps between s, p orbitals of C and s state of Zn suggest the formation of a Zn−C bond and stabilize the adsorbed methyl. This observation is in accordance with previous reports that the heterolytic dissociation of the C−

DOI: 10.1021/jacs.6b04446
J. Am. Chem. Soc. 2016, 138, 10191−10198

H bond in CH_4 could be enhanced by the electron-donation interaction between CH_4-σ(C−H) and Zn 4s.[18]

C−C Coupling from − CH_3 and CO_2. Starting from the coadsorbed methyl and H atom on the zinc center and the surface oxygen site, respectively, we mapped out the C−C coupling pathway by introducing CO_2. The highly oxidized carbon of CO_2 makes its insertion into the M−C bonds likely initiated by the nucleophilic attack.[33] Figure 4 shows the transition state of the C atom of the adsorbed methyl with the approaching CO_2.

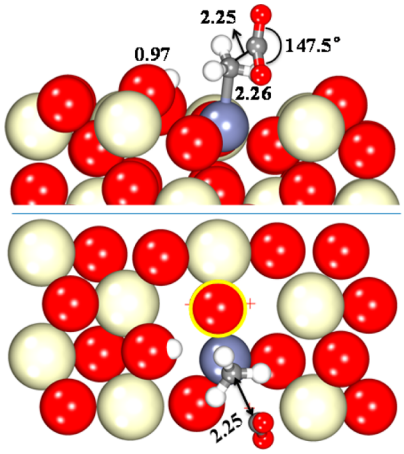

Figure 4. Transition state of C−C coupling. Side and top views are given from top to bottom. Distances are in Å.

In this transition state, the CO_2 molecule is bent from its linear configuration, with a ∠OCO angle of 147.5°. Meanwhile, both C−O bonds are elongated, to 1.19 and 1.24 Å, respectively, from their gas phase value of 1.17 Å. In this process, the O atom (with the yellow circle) stays almost at the same position as that in Figure 2. The Zn−C distance increases by 0.18 Å to 2.26 Å. Consequently, the C atom tends to lose its sp^3 hybridization as indicated by the planar nature of the three H atoms and C. On the other hand, the hydroxyl group was not affected, remaining in the same position with the same bond length of 0.97 Å. In the transition state, the distance between the two C atoms reaches a value of 2.25 Å and activation of CO_2 occurs via the orbital interaction between CO_2 and the Zn−CH_3 complex as plotted in Figure 5 of the projected density of states. As shown in Figure 5, overlaps between the s state of Zn and the s, p states of the two C atoms indicate the formation of the three-center bond in the Zn−C−C moiety.

The formation of the Zn−C−C moiety indicated that the activated CO_2 can insert into the Zn−C bond of zinc−methyl species to form a C−C bond. This heterogeneously catalyzed process has its analogue in organometallics where carboxylic acid or its derivatives could be synthesized through the carboxylation from alkylzinc reagents and CO_2.[20b−d]

Unlike typical insertion of CO_2 into M−C bond via a four-centered transition state, in which M−O and C−C bonds are being formed simultaneously with breaking the M−C bond,[17d,e] CO_2 inserts into the Zn−C bond via a S_E2 mechanism through CO_2 attacking the methyl species from the open side of the Zn−CH_3 bond. This observation is consistent with insertions of CO_2 into Pd−CH_3[34] and Ni−CH_3.[17f] Also, in the transition state, the nearly coplanar structure of CH_3 is in line with CO_2 insertion into Ni−CH_3.[17f]

According to the homogeneous-based catalysis studies, the properties of the ligands, the interaction mechanism in the transition state, the M−CH_3 bond strength, and the electrophilicity of CO_2 could all influence the C−C coupling.[17a−e,35] The enhancement of nucleophilicity of Zn−CH_3 species could facilitate a facile insertion step. The oxygen vacancies on the catalyst surface increase the electron density at the metal center. For the Zn−CH_3 species, the carbon center of CH_3 has a net charge of −0.34|e| compared to that in the CH_4 molecule. Moreover, the relaxed Zn−CH_3 bond length (2.08 Å) is longer than that reported in the reference (1.93 Å).[18a] The high electron density of Zn−CH_3 species and longer Zn−C bond length are consistent with having a methyl group with a longer M−CH_3 distance. A metal center with high electron density is expected to have an enhanced reactivity toward CO_2.[17a,c] In fact, our results show that the activation barrier of C−C coupling is only 0.51 eV on the Zn-doped ceria (111) surface. In this case, the doped Zn atom acted as an active center for the coupling reaction and can be viewed as a single-atom catalyst.[36] Despite following the same S_E2 mechanism, the activation barriers for CO_2 insertion into

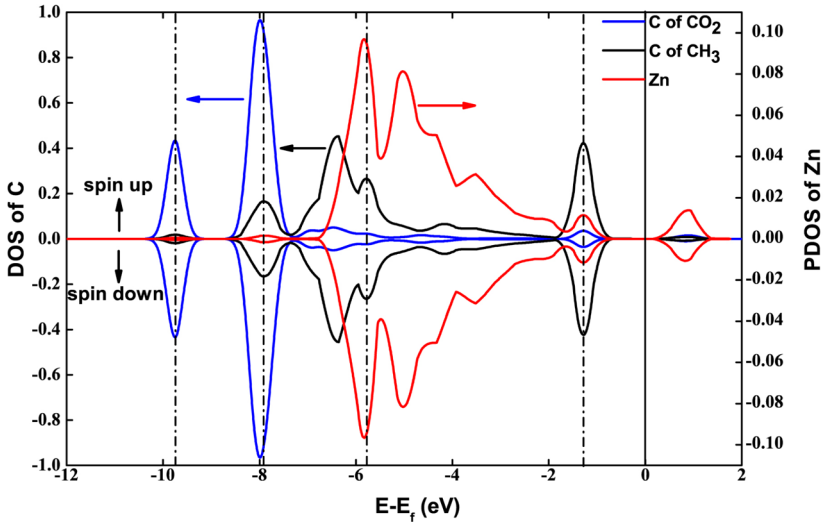

Figure 5. PDOS of Zn (red line), DOS of C of CO_2 (blue line), and C of CH_3 (black line). The solid line represents the Fermi level, and the dotted dash lines indicate the overlaps among these three atoms.

DOI: 10.1021/jacs.6b04446
J. Am. Chem. Soc. 2016, 138, 10191−10198

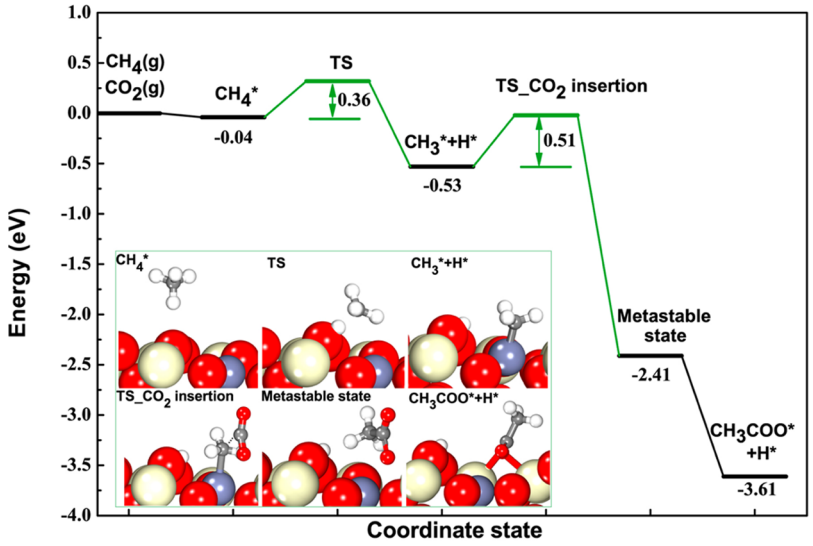

Figure 6. Potential energy profile from gaseous CH_4 and CO_2 to acetate species through C−C coupling. A* represents the adsorption state of species A on the surface.

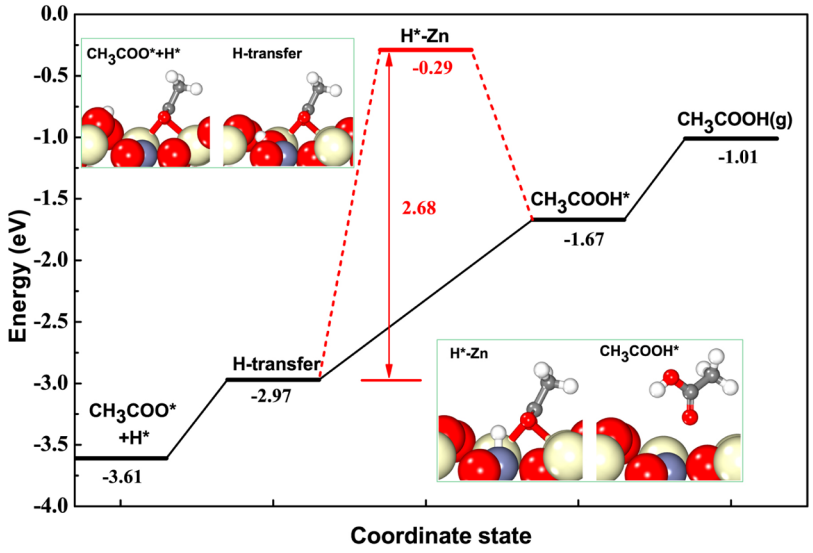

Figure 7. Potential energy profile from acetate species to acetic acid. A* represents the adsorption state of species A on the surface.

$Pd-CH_3$ and $Ni-CH_3$ are 0.83 and 1.32 eV, respectively,[17f,34] significantly higher than that for insertion into $Zn-CH_3$.

We note that this energy included the zero-point energy correction but not van der Waals (vdW) effect. Ye and co-workers showed that the reaction energy and activation barrier of an elementary step remained almost the same with and without including van der Waals corrections.[37] This low activation barrier indicates that coupling the C atom of the Zn-bound methyl species and CO_2 is feasible. Although the $Zn-CH_3$ species is not surrounded by bulky ligands, which may donate electrons to improve the reactivity of the M−C bond,[17c] the S_E2 mechanism resulted in a large ∠ZnCC angle of 125.4°. This large Zn−C−C angle, together with the sufficient overlaps between orbitals, resulted in a lower activation barrier than the previously reported value for insertion into the Cu^I-CH_3 bond.[17d] Moreover, the transition metals employed previously, including Pd, Ni, Cu, Ir, and Rh, have higher electronegativity than Zn.

Direct C−C coupling through insertion of CO_2 into Zn−C σ-bond leads to the formation of an acetate species which adsorbs on the surface in the form of a bidentate pincer through two O atoms interacting with the surface Ce atoms, at O−Ce distances of 2.63 and 2.80 Å, respectively. The reaction pathway from CH_4 (g) and CO_2 (g) to acetate species is given in Figure 6.

As shown in Figure 6, methyl is stabilized as zinc−methyl complex after overcoming a barrier of 0.36 eV. The barrier for forming the C−C bond by coupling the methyl species and CO_2 is 0.51 eV, indicating a superior catalytic activity of the active site. Once the acetate species is formed, it transforms to a state where the acetate species lies parallel to the surface. The insertion step is irreversible due to the strong exothermicity of 3.08 eV. The migration of O atom (marked with the yellow circle) contributes −1.23 eV. According to this mechanism, CO_2 comes from gas phase, making the overall reaction of CH_4 and CO_2 follow an Eley−Rideal mechanism.[38]

Formation of the Product. *Production of Aldehyde.* Acetate species is reported as a very stable intermediate, up to 500 K before decomposing or desorbing.[39] Thus, protonation or deoxygenation of the acetate species is a challenge. We

DOI: 10.1021/jacs.6b04446
J. Am. Chem. Soc. 2016, 138, 10191−10198

investigated the possible reaction pathways of producing CH_3CHO^* or CH_3COOH^* from coadsorbed CH_3COO^* and H^*. The relaxed structures are provided in Table S1 in Supporting Information.

Since the deoxygenation of acetate species to CH_3CO^* is inhibited due to the strong C−O bond, we explored hydrogen-assisted reaction pathway of forming CH_3CHO^* from CH_3COO^*. Our results showed that an energy cost of 2.58 eV is needed to hydrogenate the acetate species to CH_3CHOO^*. The following deoxygenation step to CH_3CHO^* is still 0.73 eV endothermic. On the other hand, if the acetate species eliminates an OH to form CH_2CHO^*, an energy of 2.55 eV is needed. The subsequent hydrogenation of CH_2CHO^* to CH_3CHO^* has a reaction energy of 0.76 eV. These results show that the direct production of aldehyde from the surface acetate species is unlikely due to the strong endothermicity of the reaction steps involved.

Production of Acetic Acid. We mapped out the potential energy profile for production of acetic acid in Figure 7. The black line in Figure 7 follows the two-step formation of acetic acid. The energy cost of transferring the proton from dissociative CH_4 adsorption to the adjacent O site is 0.64 eV. The following combination of the acetate species with the proton to adsorbed acetic acid is 1.30 eV endothermic. We also considered the possibility of transferring the proton to the zinc site before adding to the acetate species to form the adsorbed acetic acid, as depicted by the red line in the figure. We note that although the reaction of the acetate species with the H* on zinc site is strongly exothermic, the high endothermic step of transferring proton to the zinc site makes this reaction pathway impossible. Therefore, the production of acetic acid from the acetate species is likely to follow the pathway shown by the black line in Figure 7. The desorption energy of CH_3COOH^* is 0.66 eV. We can see from these results that the steps involved in acetic acid formation from the acetate species are all endothermic. These steps will likely impede the turnover from the reactants to the product. In practical implementation, this reaction may be coupled with the oxidation of CH_4, which would provide the needed energy for the production of acetic acid from CO_2 and CH_4.

We point out that the catalyst we used has an energy variation of 1.23 eV during the reaction process, attributed to oxygen vacancy activation. Before this step was taken into account, the overall reaction energy from CH_4 and CO_2 to acetic acid is −1.01 eV. When this energy is included in the calculation, the overall reaction energy from gas phase CH_4 and CO_2 to a gaseous acetic acid is 0.22 eV, consistent with the standard thermodynamic data.

Catalytic Cycle of C−C Coupling. The complete catalytic cycle of Zn-doped ceria catalyzed C−C coupling is shown in Scheme 1.

As shown in Scheme 1, methyl is stabilized as zinc−methyl complex following dissociative adsorption of CH_4. Gaseous CO_2 attacks the Zn−CH_3 species from the open side, resulting into a three-centered Zn−C−C moiety and making the insertion of CO_2 into Zn−C σ-bond a S_E2 mechanism. The barrier for the coupling step is 0.51 eV. The resulting acetate species from the coupling reaction is very stable, and its desorption in the form of acetic acid by reacting with the proton from CH_4 dissociation is highly endothermic. To help the process, the labeled O atom needs to be activated from its original position. This activation step overcomes a potential of 1.23 eV. The active oxygen vacancy makes the reaction from CH_4 and CO_2 to acetic acid exothermic.

Scheme 1. Catalytic Cycle of Production of CH_3COOH from CH_4 and CO_2 through Zn-Doped Ceria Catalyzed C−C Coupling[a]

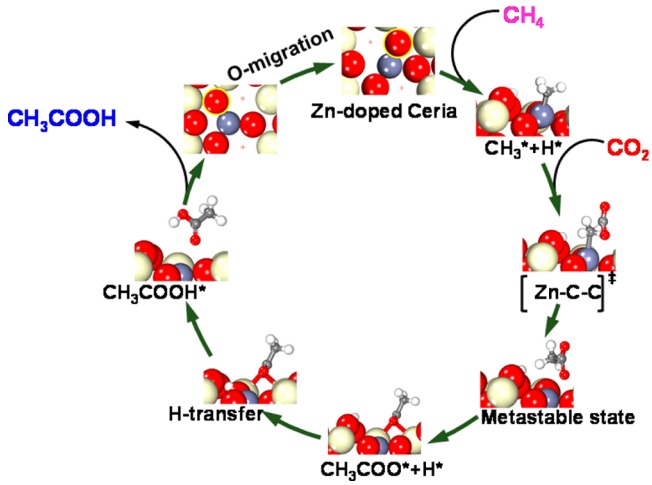

[a]A* represents the adsorption state of species A on the surface.

On the other hand, the overall reaction energy from CH_4 and CO_2 to CH_3COOH is still 0.22 eV.

So far we have only considered the possibilities of producing aldehyde and acetic acid following the formation of the acetate species. We understand that other routes may exist which result in dry re-forming products or C_2 compounds. For example, CO_2 has been used as a re-forming reagent for methane to produce syngas. We calculated the reaction of CO_2 with oxygen vacancy to form adsorbed CO (Zn−CO) or gaseous CO, with O of CO_2 filling the vacancy. The results show that both reactions are endothermic at values of 0.49 and 0.76 eV, respectively. The generated CO may desorb as a product of re-forming reaction or couple with zinc−methyl species to form the acetyl species. The acetyl species could then combine with either the surface hydroxyl to produce acetic acid or surface hydrogen to form acetaldehyde. If methylene could be stabilized on the surface and reacted with the methyl species, an ethyl-derived product such as ethanol could be the likely product. Moreover, aldehyde and ethanol may be produced from hydrogenation and deoxygenation of acetic acid. In the present study, we focused on the direct coupling reaction of the activated CH_4 with CO_2 and examined the possible products as a consequence of the initial coupling. These results allowed us to develop some preliminary understanding of the complex mechanism of catalytic CO_2 and CH_4 conversion beyond syngas production.

Effect of Metal Dopants on C−C Coupling. We examine other metals, including Al, Cd, In, and Ga, as dopant in ceria to catalyze the C−C coupling reaction. These metals are either in the same group with zinc or in the neighboring group in the periodic table. We summarized the results with the structural parameter involved in the reaction in Table 1, and the individual structures are provided in Figure S1.

On different M (Al, Zn, Cd, In, and Ga) doped ceria surface, the CO_2 molecule in all these transition states is activated to almost the same extent. As discussed in the case of Zn-doped ceria, CO_2 is activated from its linear configuration, with two differently elongated C−O bonds. One of the C−O bonds shares the same value of 1.19 Å, and the other one is in the range of 1.23−1.24 Å. Moreover, the ∠OCO angle of the activated CO_2 is in the range of 145−150°. The CO_2 molecule shared a similar V-

DOI: 10.1021/jacs.6b04446
J. Am. Chem. Soc. 2016, 138, 10191−10198

Table 1. Geometric Parameters and Calculated Results of Transition States of C−C Coupling over Different M (Al, Zn, Cd, In, and Ga) Doped Ceria Catalysts

	ion				
parameter	Al	Zn	Cd	In	Ga
C−O distance (Å)	1.19/1.23	1.19/1.24	1.19/1.23	1.19/1.24	1.19/1.24
O−C−O angle (deg)	148.9	147.5	148.7	146.9	147.1
M−C distance (Å)	2.43	2.26	2.38	2.49	2.33
C−C distance (Å)	2.32	2.25	2.23	2.17	2.18
ion radius (Å)	0.54	0.74	0.95	0.80	0.62
electronegativity	1.61	1.65	1.69	1.78	1.81
TS energy (eV)	0.37	0.51	0.92	1.11	1.21

shaped structure. However, the M−C and C−C distances in the transition states are different from each other. In addition, the activation barriers are different, with values of 0.37 eV, 0.51 eV, 0.92 eV, 1.11 eV, and 1.21 eV for Al, Zn, Cd, Ga, and In, respectively.

The M−C distance in the transition state ranges from 2.26 to 2.49 Å and can be correlated with the ionic radius to some degree. As shown in Table 1, the Al-, Zn-, and Cd-doped ceria catalysts follow a general trend that the C−C distance decreases as the barrier increases. In fact, on Ga-doped ceria surface, the activation barrier is 0.1 eV higher than that on In-doped ceria surface. However, the C−C distance on Ga-doped ceria is 2.18 Å, slightly longer than that on In-doped ceria. These results demonstrate that the variation of activation barrier is reflected in the C−C distance in transition state. Further analysis of the results showed that the activation barrier correlates with the electronegativity of the doped metal. The correlation between the C−C coupling barrier and the electronegativity is plotted in Figure 8.

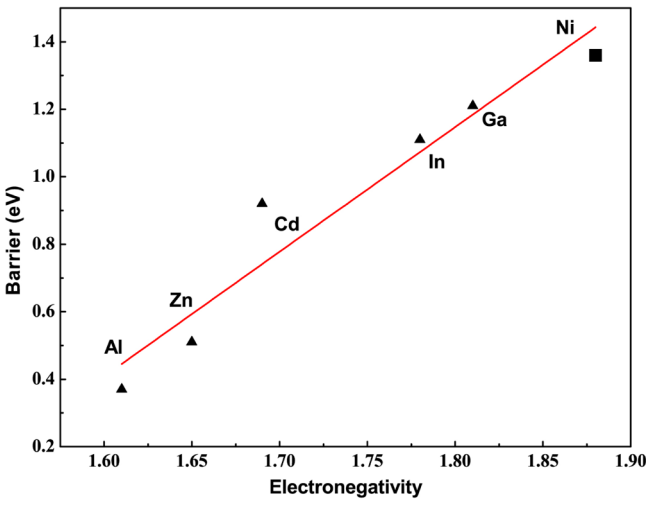

Figure 8. Dependence of the C−C coupling barrier on the electronegativity of the dopants (Al, Zn, Cd, In, and Ga).

As shown in Figure 8, the activation barrier for C−C coupling increases as the electronegativity of the doped metal increases. This can be understood from the fact that methyl is stabilized on the surface through the M−C bond. The strength of the M−C bond is expected to be high if the metal has a high electronegativity. The stronger M−C bond will in turn reduce nucleophilicity of methyl group, resulting in an increased activation barrier for the coupling reaction. This is reflected in the calculated CO_2−CH_3 coupling barrier of 1.36 eV by assuming that CH_3 could be stabilized on the Ni-doped ceria. We also plotted the coupling barrier on Ni-doped ceria against the electronegativity of Ni in Figure 8 and found that the linear correlation remained valid. However, doping transition metals would also result in an enhanced dehydrogenation activity. For example, the activation of methane on the Ni-doped ceria to form Ni-CH_3 and coadsorbed H is highly exothermic, with a reaction energy of −1.94 eV. Further dehydrogenation of CH_3 to CH_2 is almost thermally neutral (0.01 eV). In contrast, the same reaction on the Zn−doped ceria is endothermic with a reaction energy of 0.53 eV, higher than the barrier of CO_2 insertion into the CH_3−Zn bond. These results indicate that CH_3 will not likely couple with CO_2 before being dehydrogenated to CH_2, and then to CH and C, consistent with the fact that Ni is a good catalyst for dry re-forming.[40] Consequently, we choose base metals instead of transition metals as the active center for the coupling reaction in the present study.

CONCLUSIONS

Zn-doped ceria catalyst was found to catalyze the coconversion of CH_4 and CO_2. Dissociative adsorption of CH_4 is thermodynamically favorable through the formation of a Zn−C bond, with an adsorption energy of −0.53 eV. Our results showed that CO_2 insertion into the Zn−C bond could be achieved under very modest conditions with an activation barrier of 0.51 eV. The insertion is initiated by CO_2 attacking the Zn−CH_3 species from the open side, suggesting a S_E2 mechanism. A three-center Zn−C−C bond is formed at the transition state, supported by the DOS analysis. The Brønsted proton generated from CH_4 dissociation could combine with the surface acetate species to form acetic acid, although the process is highly endothermic. We also showed that other dopants can also make ceria active for the coupling reaction and the activation barrier correlates with the electronegativity of the doped metal. The present study predicts the possibility of realizing direct C−C coupling between activated CH_4 and CO_2 on heterogeneous catalysts and will have positive impact on the utilization of the greenhouse gases, if implemented in practice.

ASSOCIATED CONTENT

Supporting Information

The Supporting Information is available free of charge on the ACS Publications website at DOI: 10.1021/jacs.6b04446.

Relaxed structures involved in the process of product desorption and relaxed structures of C−C coupling on Al-, Cd-, Ga-, and In-doped ceria (PDF)

DOI: 10.1021/jacs.6b04446
J. Am. Chem. Soc. 2016, 138, 10191−10198

AUTHOR INFORMATION

Corresponding Authors

*X.Z.: xinlizhu@tju.edu.cn

*Q.G.: qge@chem.siu.edu

Notes

The authors declare no competing financial interest.

ACKNOWLEDGMENTS

We acknowledge the support of the National Natural Science Foundation of China (Grants 21373148, 21206116, 21276191, and 21076152). Q.G. acknowledges the support of NSF-CBET program (Award CBET-1438440). The high performance computing center of Tianjin University managed and provided major computing resources for this work.

REFERENCES

(1) (a) Yu, K. M.; Curcic, I.; Gabriel, J.; Tsang, S. C. *ChemSusChem* **2008**, *1*, 893. (b) Aresta, M.; Dibenedetto, A. *Dalton Trans.* **2007**, 2975.

(2) Metz, B., Davidson, O., de Coninck, H., Loos, M., Meyer, L.; Eds. *Carbon Dioxide Capture and Storage*; Cambridge University Press: New York, 2005.

(3) Angamuthu, R.; Byers, P.; Lutz, M.; Spek, A. L.; Bouwman, E. *Science* **2010**, *327*, 313.

(4) (a) Varghese, O. K.; Paulose, M.; Latempa, T. J.; Grimes, C. A. *Nano Lett.* **2009**, *9*, 731. (b) Sato, S.; Arai, T.; Morikawa, T.; Uemura, K.; Suzuki, T. M.; Tanaka, H.; Kajino, T. *J. Am. Chem. Soc.* **2011**, *133*, 15240.

(5) (a) Graciani, J.; Mudiyanselage, K.; Xu, F.; Baber, A. E.; Evans, J.; Senanayake, S. D.; Stacchiola, D. J.; Liu, P.; Hrbek, J.; Fernandez Sanz, J.; Rodriguez, J. A. *Science* **2014**, *345*, 546. (b) An, X.; Li, J.; Zuo, Y.; Zhang, Q.; Wang, D.; Wang, J. *Catal. Lett.* **2007**, *118*, 264. (c) Huff, C. A.; Sanford, M. S. *J. Am. Chem. Soc.* **2011**, *133*, 18122. (d) Menard, G.; Stephan, D. W. *J. Am. Chem. Soc.* **2010**, *132*, 1796. (e) Courtemanche, M. A.; Legare, M. A.; Maron, L.; Fontaine, F. G. *J. Am. Chem. Soc.* **2014**, *136*, 10708.

(6) (a) Harshini, D.; Lee, D. H.; Kim, Y.; Nam, S. W.; Han, J. H.; Ham, H. C.; Yoon, C. W. *Catal. Lett.* **2014**, *144*, 656. (b) Faria, E. C.; Neto, R. C. R.; Colman, R. C.; Noronha, F. B. *Catal. Today* **2014**, *228*, 138. (c) Kambolis, A.; Matralis, H.; Trovarelli, A.; Papadopoulou, C. *Appl. Catal., A* **2010**, *377*, 16.

(7) (a) Pham, M. H.; Goujard, V.; Tatibouët, J. M.; Batiot-Dupeyrat, C. *Catal. Today* **2011**, *171*, 67. (b) Zhang, X.; Dai, B.; Zhu, A.; Gong, W.; Liu, C. *Catal. Today* **2002**, *72*, 223.

(8) (a) Banerjee, A.; Dick, G. R.; Yoshino, T.; Kanan, M. W. *Nature* **2016**, *531*, 215. (b) Beckman, E. J. *Nature* **2016**, *531*, 180.

(9) (a) Wu, J. F.; Yu, S. M.; Wang, W. D.; Fan, Y. X.; Bai, S.; Zhang, C. W.; Gao, Q.; Huang, J.; Wang, W. *J. Am. Chem. Soc.* **2013**, *135*, 13567. (b) Ding, Y.-H.; Huang, W.; Wang, Y.-G. *Fuel Process. Technol.* **2007**, *88*, 319.

(10) Nizova, G. V.; Shul'pin, G. B.; Nizova, G. V.; Süss-Fink, G.; Stanislas, S. *Chem. Commun.* **1998**, 1885.

(11) Kurioka, M.; Nakata, K.; Jintoku, T.; Taniguchi, Y.; Takaki, K.; Fujiwara, Y. *Chem. Lett.* **1995**, 244.

(12) Huang, W.; Xie, K. C.; Wang, J. P.; Gao, Z. H.; Yin, L. H.; Zhu, Q. M. *J. Catal.* **2001**, *201*, 100.

(13) Wilcox, E. M.; Roberts, G. W.; Spivey, J. J. *Catal. Today* **2003**, *88*, 83.

(14) Huang, W.; Zhang, C.; Yin, L.; Xie, K. *J. Nat. Gas Chem.* **2004**, *13*, 113.

(15) Ding, Y.-H.; Huang, W.; Wang, Y.-G. *Fuel Process. Technol.* **2007**, *88*, 319.

(16) Liu, C.-j.; Li, Y.; Zhang, Y.-p.; Wang, Y.; Zou, J.; Eliasson, B.; Xue, B. *Chem. Lett.* **2001**, 1304.

(17) (a) Darensbourg, D. J.; Groetsch, G.; Wiegreffe, P.; Rheingold, A. L. *Inorg. Chem.* **1987**, *26*, 3827. (b) Darensbourg, D. J.; Hanckel, R. K.; Bauch, C. G.; Pala, M.; Simmons, D.; White, J. N. *J. Am. Chem. Soc.* **1985**, *107*, 7463. (c) Johansson, R.; Jarenmark, M.; Wendt, O. F. *Organometallics* **2005**, *24*, 4500. (d) Sakaki, S.; Ohkubo, K. *Inorg. Chem.* **1989**, *28*, 2583. (e) Holl, M. M.; Hillhouse, G. L.; Folting, K.; Huffman, J. C. *Organometallics* **1987**, *6*, 1522. (f) Schmeier, T. J.; Hazari, N.; Incarvito, C. D.; Raskatov, J. A. *Chem. Commun.* **2011**, *47*, 1824.

(18) (a) Oda, A.; Torigoe, H.; Itadani, A.; Ohkubo, T.; Yumura, T.; Kobayashi, H.; Kuroda, Y. *J. Phys. Chem. C* **2013**, *117*, 19525. (b) Oda, A.; Torigoe, H.; Itadani, A.; Ohkubo, T.; Yumura, T.; Kobayashi, H.; Kuroda, Y. *J. Phys. Chem. C* **2014**, *118*, 15234.

(19) Panjan, W.; Sirijaraensre, J.; Warakulwit, C.; Pantu, P.; Limtrakul, J. *Phys. Chem. Chem. Phys.* **2012**, *14*, 16588.

(20) (a) Yeung, C. S.; Dong, V. M. *J. Am. Chem. Soc.* **2008**, *130*, 7826. (b) Ochiai, H.; Jang, M.; Hirano, K.; Yorimitsu, H.; Oshima, K. *Org. Lett.* **2008**, *10*, 2681. (c) Metzger, A.; Bernhardt, S.; Manolikakes, G.; Knochel, P. *Angew. Chem., Int. Ed.* **2010**, *49*, 4665. (d) Kobayashi, K.; Kondo, Y. *Org. Lett.* **2009**, *11*, 2035.

(21) Sattler, W.; Parkin, G. *J. Am. Chem. Soc.* **2011**, *133*, 9708.

(22) Cheng, Z.; Sherman, B. J.; Lo, C. S. *J. Chem. Phys.* **2013**, *138*, 014702.

(23) (a) Kresse, G.; Hafner, J. *Phys. Rev. B: Condens. Matter Mater. Phys.* **1993**, *48*, 13115. (b) Kresse, G.; Furthmüller, J. *Phys. Rev. B: Condens. Matter Mater. Phys.* **1996**, *54*, 11169.

(24) Perdew, J. P.; Burke, K.; Ernzerhof, M. *Phys. Rev. Lett.* **1996**, *77*, 3865.

(25) Cheng, L.; Mei, D.; Ge, Q. *J. Phys. Chem. C* **2009**, *113*, 18296.

(26) (a) Mayernick, A. D.; Janik, M. J. *J. Catal.* **2011**, *278*, 16. (b) Mayernick, A. D.; Janik, M. J. *J. Phys. Chem. C* **2008**, *112*, 14955. (c) Krcha, M. D.; Mayernick, A. D.; Janik, M. J. *J. Catal.* **2012**, *293*, 103. (d) Dholabhai, P. P.; Adams, J. B.; Crozier, P.; Sharma, R. *J. Chem. Phys.* **2010**, *132*, 094104. (e) Vecchietti, J.; Bonivardi, A.; Xu, W.; Stacchiola, D.; Delgado, J. J.; Calatayud, M.; Collins, S. E. *ACS Catal.* **2014**, *4*, 2088.

(27) (a) Kresse, G.; Joubert, D. *Phys. Rev. B: Condens. Matter Mater. Phys.* **1999**, *59*, 1758. (b) Blöchl, P. E. *Phys. Rev. B: Condens. Matter Mater. Phys.* **1994**, *50*, 17953.

(28) (a) Kümmerle, E. A.; Heger, G. *J. Solid State Chem.* **1999**, *147*, 485. (b) Vilé, G.; Dähler, P.; Vecchietti, J.; Baltanás, M.; Collins, S.; Calatayud, M.; Bonivardi, A.; Pérez-Ramírez, J. *J. Catal.* **2015**, *324*, 69.

(29) Hsu, L.-C.; Tsai, M.-K.; Lu, Y.-H.; Chen, H.-T. *J. Phys. Chem. C* **2013**, *117*, 433.

(30) Knapp, D.; Ziegler, T. *J. Phys. Chem. C* **2008**, *112*, 17311.

(31) Ye, J.; Liu, C.; Mei, D.; Ge, Q. *ACS Catal.* **2013**, *3*, 1296.

(32) Patil, U.; Saih, Y.; Abou-Hamad, E.; Hamieh, A.; Pelletier, J. D.; Basset, J. M. *Chem. Commun.* **2014**, *50*, 12348.

(33) Fan, T.; Chen, X.; Lin, Z. *Chem. Commun.* **2012**, *48*, 10808.

(34) Johnson, M. T.; Johansson, R.; Kondrashov, M. V.; Steyl, G.; Ahlquist, M. S.; Roodt, A.; Wendt, O. F. *Organometallics* **2010**, *29*, 3521.

(35) Mankad, N. P.; Gray, T. G.; Laitar, D. S.; Sadighi, J. P. *Organometallics* **2004**, *23*, 1191.

(36) Yang, X.-F.; Wang, A.; Qiao, B.; Li, J.; Liu, J.; Zhang, T. *Acc. Chem. Res.* **2013**, *46*, 1740.

(37) Ye, J.; Liu, C.; Ge, Q. *Phys. Chem. Chem. Phys.* **2012**, *14*, 16660.

(38) Zhang, R.; Song, L.; Liu, H.; Wang, B. *Appl. Catal., A* **2012**, *443–444*, 50.

(39) Calaza, F. C.; Chen, T.-L.; Mullins, D. R.; Xu, Y.; Overbury, S. H. *Catal. Today* **2015**, *253*, 65.

(40) Liu, Z.; Grinter, D. C.; Lustemberg, P. G.; Nguyen-Phan, T. D.; Zhou, Y.; Luo, S.; Waluyo, I.; Crumlin, E. J.; Stacchiola, D. J.; Zhou, J.; Carrasco, J.; Busnengo, H. F.; Ganduglia-Pirovano, M. V.; Senanayake, S. D.; Rodriguez, J. A. *Angew. Chem., Int. Ed.* **2016**, *55*, 7455.

DOI: 10.1021/jacs.6b04446
J. Am. Chem. Soc. 2016, 138, 10191–10198